Molecules and Cells

UHRF1 Induces Methylation of the *TXNIP* Promoter and Down-Regulates Gene Expression in Cervical Cancer

Min Jun Kim[1], Han Ju Lee[1], Mee Young Choi[1], Sang Soo Kang[1], Yoon Sook Kim[1], Jeong Kyu Shin[2], and Wan Sung Choi[1,*]

[1]Department of Anatomy and Convergence Medical Science, Institute of Health Sciences, College of Medicine, Gyeongsang National University, Jinju 52727, Korea, [2]Department of Obstetrics and Gynecology, College of Medicine, Gyeongsang National University, Jinju 52727, Korea
*Correspondence: choiws@gnu.ac.kr
https://doi.org/10.14348/molcells.2021.0001
www.molcells.org

DNA methylation, and consequent down-regulation, of tumour suppressor genes occurs in response to epigenetic stimuli during cancer development. Similarly, human oncoviruses, including human papillomavirus (HPV), up-regulate and augment DNA methyltransferase (DNMT) and histone deacetylase (HDAC) activities, thereby decreasing tumour suppressor genes (TSGs) expression. Ubiquitin-like containing PHD and RING finger domain 1 (UHRF1), an epigenetic regulator of DNA methylation, is overexpressed in HPV-induced cervical cancers. Here, we investigated the role of UHRF1 in cervical cancer by knocking down its expression in HeLa cells using lentiviral-encoded short hairpin (sh)RNA and performing cDNA microarrays. We detected significantly elevated expression of thioredoxin-interacting protein (TXNIP), a known TSG, in UHRF1-knockdown cells, and this gene is hypermethylated in cervical cancer tissue and cell lines, as indicated by whole-genome methylation analysis. Up-regulation of UHRF1 and decreased TXNIP were further detected in cervical cancer by western blot and immunohistochemistry and confirmed by Oncomine database analysis. Using chromatin immunoprecipitation, we identified the inverted CCAAT domain-containing UHRF1-binding site in the *TXNIP* promoter and demonstrated UHRF1 knockdown decreases UHRF1 promoter binding and enhances TXNIP expression through demethylation of this region. *TXNIP* promoter CpG methylation was further confirmed in cervical cancer tissue by pyrosequencing and methylation-specific polymerase chain reaction. Critically, down-regulation of UHRF1 by siRNA or UHRF1 antagonist (thymoquinone) induces cell cycle arrest and apoptosis, and ubiquitin-specific protease 7 (USP7), which stabilises and promotes UHRF1 function, is increased by HPV viral protein E6/E7 overexpression. These results indicate HPV might induce carcinogenesis through UHRF1-mediated *TXNIP* promoter methylation, thus suggesting a possible link between CpG methylation and cervical cancer.

Keywords: cervical cancer, DNA methylation, epigenetic modulator, TXNIP, UHRF1

INTRODUCTION

Epigenetic changes, including DNA methylation and histone modification, play prominent roles in the oncogenesis of solid tumours and haematological malignancies (Esteller, 2008; Poreba et al., 2011; Yu, 2008). As such, many viral infections promote carcinogenesis via oncoviral protein-mediated inter-

Received 3 January, 2021; revised 16 February, 2021; accepted 21 February, 2021; published online 26 March, 2021

eISSN: 0219-1032

ference with the host cell epigenetic machinery (Poreba et al., 2011). Epigenetic effector molecules targeted by oncogenic viruses therefore represent appealing targets for preventing and treating virus-induced malignancies (El-Araby et al., 2016).

DNA methylation is mediated by a complex of three protein subunits: DNA methyltransferase 1 (DNMT1), ubiquitin-like containing PHD and RING finger domain 1 (UHRF1), and ubiquitin-specific protease 7 (USP7) (Beck et al., 2018; Felle et al., 2011). UHRF1, also known as inverted CCAAT box-binding protein (ICBP90), epigenetically regulates DNA methylation by recruiting the methyltransferase DNMT1(Bostick et al., 2007; Sharif et al., 2007) and links DNA methylation and methylation maintenance following cell division (Bostick et al., 2007; Sheng et al., 2016). USP7, also known as HAUSP, is a member of the deubiquitinating enzyme family that prevents UHRF1 degradation and maintains DNA methylation by forming a trimeric complex with DNMT1 and UHRF1. USP7 promotes virus-induced epigenetic modification of host genomes, thereby regulating the life cycle of viruses such as herpesvirus and Epstein–Barr virus (Lindner, 2007). Various viruses, including human papilloma virus (HPV), induce USP7 expression and DNMT1 stabilisation. UHRF1 inhibits tumour suppressor genes (TSGs) through promoter methylation, allowing cancer cells to escape cell cycle arrest and apoptosis (Gronbaek et al., 2007). UHRF1 is overexpressed in several types of cancer, including bladder, prostate, lung, and cervical cancers (Alhosin et al., 2011; Babbio et al., 2012; Ge et al., 2016; Unoki et al., 2009; Wan et al., 2016).

Thioredoxin-interacting protein (TXNIP), also known as vitamin D3 up-regulated protein 1 (VDUP-1), is a key regulator of the redox scavenger system. This protein binds thioredoxin (Trx1), inhibiting its anti-oxidative function (Hong et al., 2016; Kaimul et al., 2007). Notably, TXNIP is frequently under-expressed in cancers lacking genetic mutations, including leukaemia and lymphoma (Erkeland et al., 2009). Hypermethylation of the *TXNIP* promoter and consequent loss or decrease of TXNIP expression were also recently identified in carcinogenesis (Dutta et al., 2005), and conversely, inhibition of tumour growth and apoptosis-induced cell cycle arrest (Dunn et al., 2010; Elgort et al., 2010; Han et al., 2003; Jeon et al., 2005; Liu and Min, 2002; Saitoh et al., 1998; Welsh et al., 2002) due to rebounding TXNIP expression were reported in renal cell carcinoma (RCC) (Jiao et al., 2019). These data suggest that *TXNIP* promoter methylation in cancer could represent an epigenetic marker for oncogenesis. However, despite evidence suggesting UHRF1 promotes cancer progression through *TXNIP* promoter methylation in RCC (Jiao et al., 2019), the epigenetic modulation of TXNIP expression by UHRF1 has not been studied in other cancers.

Here, we investigated the epigenetic regulation of TXNIP by UHRF1 in cervical cancer. To identify oncogenic markers, we constructed stable UHRF1-knockdown HeLa cells and performed cDNA microarray analysis. Whole-genome methylation assays showed that *TXNIP* was significantly overexpressed in UHRF1-knockdown cells and hypermethylated in cancer. Increased UHRF1 and decreased TXNIP protein levels were observed in cervical cancer tissue by western blot, immunohistochemistry, and Oncomine database analysis. UHRF1 binding to the *TXNIP* promoter was confirmed by chromatin immunoprecipitation (ChIP) and methylation was confirmed by hypermethylation pyrosequencing and methylation-specific polymerase chain reaction (PCR). We further showed that down-regulation of UHRF1 promoted cell cycle arrest and apoptosis, and overexpression of HPV E6/E7 induced ubiquitin-specific protease 7 (USP7), which promoted UHRF1 function, leading to TXNIP inhibition. Our studies suggest that TXNIP is a novel target of UHRF1 that is overexpressed in HPV-induced cervical cancer.

MATERIALS AND METHODS

Cell culture and treatment

HeLa (ATCC Cat. #CCL-002, HPV-18-positive), SiHa (ATCC Cat. #HTB-35, HPV-16-positive), and C-33A (ATCC Cat. #HTB-31, HPV-negative) cervical cancer cell lines, as well as retinal pigment epithelial (ATCC Cat. #CRL-2302, ARPE-19), and HPV16 E6/E7-transformed human epidermal keratinocyte (ATCC Cat. #CRL-2404, HEK001) cell lines, were purchased from the American Type Culture Collection (ATCC, USA). Human keratinocyte (Accegen Cat. #ABC-TC536S, HaCaT) was purchased from Accegen Biotechnology (USA). HeLa and HaCaT cells were maintained in Dulbecco's modified Eagle medium (DMEM; Gibco BRL, USA). SiHa and C33A cells were maintained in Minimum Essential Medium (Gibco BRL). HEK001 cells were cultured in Keratinocyte-Serum-Free Medium (Gibco BRL), with 5 ng/ml human recombinant epidermal growth factor (EGF) and 2 mM L-glutamine (provided in kit), and ARPE-19 cells were grown in DMEM-Ham's F12 media (Gibco BRL). All cell line lines were routinely tested for microbial contamination and monitored for mycoplasma contamination by PCR detection (Lookout Mycoplasma PCR Detection Kit, Cat. #MP0035-1KT; Sigma-Aldrich, USA) within 6 months of being thawed.

For 5-aza-deoxycytidine (5azadC) or Trichostatin A (TSA) treatment, HeLa cells were seeded in 100-mm dishes at 1 × 10^6 cells/dish and adhered overnight at 37°C. Cells were then were treated with 0.1% DMSO as a control, 10 μM 5azadC, or 1 μM TSA for 24 h at 37°C.

Transfection of shRNA-expressing lentiviral particles for stable UHRF1 knockdown

Short hairpin (sh)RNA targeting *UHRF1* (shUHRF1; sc-76805-v) and control shRNA (shCTL; sc-108080) were purchased from Santa Cruz Biotechnology (USA). For transfections, HeLa cells were grown to approximately 50% confluence in 24-well plates and infected with virus supernatants at a multiplicity of infection of 10, with 5 μg/ml Polybrene (sc-134220; Santa Cruz Biotechnology) overnight. Culture medium was then removed and replaced with 1 ml complete medium, without Polybrene, for 24 h, and HeLa cells stably expressing shRNA were selected by puromycin (10 μg/ml) treatment for two weeks.

Patient tumour samples

Human cervical tissues were collected from patients undergoing cervical biopsies and loop electrosurgical excision

procedures. All patients were high-risk HPV16/18-positive and between 29 and 84 years of age (mean, 57.1 years). Tissue samples from normal subjects (n = 3) or cervical cancer patients (n = 22) were used for western blot analysis, pyrosequencing and methylation-specific PCR. Informed consent was obtained from all participants, and the study was approved by the Ethics Committee of Gyeongsang National University Hospital (IRB No.2014-10-024-001).

RNA isolation and microarray analysis

Global gene expression analyses using Affymetrix GeneChip® Human Gene 2.0 ST oligonucleotide arrays were performed by the commercial microarray service Ebiogen (Korea). Total RNAs from shCTL HeLa cells and shUHRF1 HeLa cells (300 ng from each sample) was converted to double-stranded cDNA using random hexamers incorporating a T7 promoter and Fragmented cDNA was generated by manufacturer's protocol (Affymetrix, USA). Fragmented end-labelled cDNA was hybridised to the array for 16 h at 45°C and 60 rpm, as described in the GeneChip Whole Transcript Sense Target Labeling Assay Manual (Affymetrix). The chip was scanned with a GeneChip Array Scanner 3000 7G (Affymetrix) and analysed using Affymetrix Command Console software, v1.1. Normalisation was performed with the Robust Multi-array Average (RMA) algorithm, implemented in Affymetrix Expression Console software, and graphs and heatmaps were prepared using the MeV program.

DNA methylation analysis with Infinium MethylationEPIC BeadChip arrays

Genomic DNA was extracted from frozen cervical tissues and cervical cancer cell lines using NucleoSpin® columns (Macherey-Nagel, Germany), and bisulfite converted with the EZ DNA Methylation Kit (Zymo Research, USA). Bisulfite-converted DNA (200 ng per sample) was used for Infinium MethylationEPIC arrays (Illumina, USA). Genomic DNA was amplified and hybridised to BeadChips from the Infinium MethylationEPIC BeadChip Kit (Illumina). Image intensities were extracted using Illumina iScan Control software, and graphs.

Oncomine database and GEO2R analysis

The Oncomine database (https://www.oncomine.org/) is an online data-mining platform, containing a collection of whole-genome microarray data, which is comprised of 715 datasets and 86,733 samples (Rhodes et al., 2004). Expression levels of *UHRF1* mRNA (log2 median-centred intensity) in cervical cancer and normal cervix were retrieved from the Pyeon multi-cancer dataset (Pyeon et al., 2007) (GSE6791), and expression levels of *TXNIP* mRNA (log2 median-centred ratio) were obtained from the Biewenga dataset (Biewenga et al., 2008) (GSE7410).

Expression levels of *TXNIP* and *USP7* mRNA were retrieved from public gene expression data in the Gene Expression Omnibus (GEO) (Barrett et al., 2013) database, using the GSE6791 (Pyeon et al., 2007) dataset. This contains expression profiles of HPV-positive and HPV-negative head/neck and cervical cancer from Affymetrix Human Genome U133 Plus 2.0 arrays (GEO accession GPL570). Only normal cervix (n = 8) and cervical cancer (n = 20) samples were extracted.

Bisulfite pyrosequencing

Bisulfite-modified genomic DNA was prepared using the EZ DNA Methylation-Lightning™ Kit, according to manufacturer instructions. Bisulfite reactions were performed on 200 ng genomic DNA; reaction volume was adjusted to 20 μl with sterile water, and 130 μl CT Conversion Reagent (Zymo Research) was added. Reactions were performed in a thermal cycler (MJ Research; Bio-Rad, USA), using the following parameters: 8 min at 98°C and 60 min at 54°C; samples were stored at 4°C for up to 20 h.

DNA was purified using reagents provided by the EZ DNA Methylation-Lightning™ Kit. Zymo-Spin ICTM Columns, containing 600 μl M-Binding Buffer, centrifuged at full speed for 30 s, flow-through was discarded, and columns were washed with 200 μl M-Wash Buffer, followed by a full-speed spin to remove buffer. After adding M-Desulphonation Buffer to each column (200 μl), they were incubated at room temperature (RT; 20°C-30°C) for 15-20 min. Columns were then washed again as described above. Converted genomic DNA was then eluted with 20 μl M-Elution Buffer, and DNA samples were stored at −20°C until further use.

Chromatin immunoprecipitation assays (ChIP)

ChIP assays were performed using the High-Sensitivity ChIP Kit (ab195913; Abcam, UK), according to manufacturer instructions. Antibodies used included the following: anti-UHRF1 (Epigentek, USA), anti-RNA polymerase II positive control (provided in the kit), or non-immune IgG negative control (provided in the kit). Primer sequences (Wei et al., 2017) are listed in Supplementary Table S1. ChIP-PCR assays were performed using the 2X FAST Q-PCR Master MIX SYBR (SMOBIO Technology, Taiwan). All data were normalised to negative control (IgG), and DNA binding enrichments were determined using the $2^{(IgG\ CT-TXNIP\ CT)}$ method.

Pyrosequencing analysis

Bisulfite pyrosequencing was used to assess methylation status of the *TXNIP* gene. Primers were designed using Pyrosequencing Assay Design Software (v2.0; Qiagen, Germany), and primer sequences are listed in Supplementary Table S2. PCR reactions were performed in a final volume of 20 μl, with 20 ng or more converted genomic DNA, PCR premixture (Enzynomics, Korea), 1 μl of 10 pmole/μl Primer-S, and 1 μl of 10 pmole/μl biotinylated-Primer-As. Amplification was conducted according to guidelines suggested by Pyrosequencing Assay Design Software.

Single-strand DNA template was prepared from 18 μl of biotinylated PCR products using Streptavidin Sepharose® High Performance beads (Amersham Biosciences, UK), following the PSQ 96 sample preparation guidelines using multichannel pipets. Sequencing reactions were performed with 15 pmol of the respective sequencing primer and run on a PyroMark ID system with the PyroMark Gold Reagents Kit (Qiagen), according to manufacturer instructions and without further optimisation. TXNIP methylation level is calculated as the average of the proportion of C (%) at the position 1 CpG sites.

Methylation-specific PCR (MSP)

Bisulfite-treated DNA (500 ng) was amplified with primers

specific for methylated and unmethylated *TXNIP* promoter. MSP primers were designed by the MethPrimer program (http://www.urogene.org/methprimer/), and all primer sequences are listed Supplementary Table S3. Reactions were performed in a thermocycler using the following parameters: 94°C for 2 min, followed by 40 cycles of 94°C for 30 s, 60°C for 30 s, and 72°C for 30 s, and a final extension at 72°C for 5 min. Bands were detected using the iBright Imaging System (Thermo Fisher Scientific, USA).

Western blot analysis

Cells and tissues were homogenised in RIPA buffer (Thermo Fisher Scientific) with protease inhibitor cocktail (Sigma-Aldrich). Protein concentrations were determined with the Pierce Bicinchoninic Acid (BCA) Protein Assay Kit (Thermo Fisher Scientific). Proteins were separated by SDS-PAGE on 8%-15% gels and transferred to nitrocellulose membranes (Millipore, USA). Blot images were captured on a RAS-4000 image reader (Fujifilm, Japan). Nuclear and cytoplasmic protein fractions were separated with the Nuclear/Cytosol Fraction Kit (Biovision, USA); density values were normalised to β-actin and analysed using Image J software. All antibodies are listed in Supplementary Table S4.

Immunocytochemistry

Tissue sections and cells were fixed on gelatine-coated slides, deparaffinised in xylene, and rehydrated in graded alcohol solution. Endogenous peroxidase activity was inhibited by incubation for 30 min in 0.3% H_2O_2 in 0.01 M Tris, and non-specific binding was reduced by blocking in 5% serum. Samples were incubated with primary antibody overnight at 4°C, and then with specific fluorescence-conjugated secondary IgG for 1 h in a light-protected chamber at RT. Sections were counterstained with 4,6-diamidino-2-phenylindole dihydrochloride (DAPI; Invitrogen, USA) and mounted. All images were obtained using a BX51-DSU fluorescence microscope (Olympus, Japan).

Terminal deoxynucleotidyl transferase dUTP nick end labelling (TUNEL) staining

HeLa cells stably expressing shCTL or shUHRF1 were seeded into 24-well plates at 2×10^4 cells per well and grown for 16 h. Apoptotic cells were measured using the *In Situ* Cell Death Detection Kit (Sigma-Aldrich), stained with TMR red (Roche Applied Science, Germany) for 15 min, and mounted on slides using ProLong Gold Antifade Mountant (Invitrogen), with DAPI nuclear staining. All images were obtained using a BX51-DSU fluorescence microscope (Olympus).

Cell proliferation assay

HeLa cells stably expressing shCTL or shUHRF1 were seeded at 1.0×10^4 cells/well in 96-well plates and treated with TQ (0, 15, 30, or 60 μM) for 24 h. MTT solution (2 mg/ml) was then added to each well, and plates were incubated at 37°C for 2 h. The resulting formazan crystals were dissolved in dimethyl sulfoxide, and absorbance was measured at 570 nm using a microplate reader (Tecan, Switzerland).

Cell cycle and apoptosis analysis

Cells were collected and seeded into 6-well plates at 1×10^5 cells per well and cultured for 16 h. These were treated with 30 μM TQ for 24 h, trypsinised, fixed with cold 90% ethanol, and incubated 1 h at 4°C. Cells were then pelleted, resuspended in 1 ml PBS, containing 1 mg/ml propidium iodide (PI) and 1 mg/ml RNase A, and incubated at 37°C for 30 min. Cell cycle (Sub-G_1) and apoptosis were determined by flow cytometry, according to manufacturer protocols (FACScan; BD Biosciences, USA), and data were analysed using CXP 2.2 software.

Statistical analysis

Data are expressed as the mean ± SEM. Statistical significance was determined using the two-tailed Student's unpaired *t*-test for comparison of two groups and ANOVA to compare multiple treatment groups (GraphPad Prism 5; GraphPad Software, USA). P values < 0.05 were considered statistically significant.

RESULTS

TXNIP is induced in shUHRF1 HeLa cells and highly methylated in cervical cancer

To identify down-stream target genes of UHRF1, an important regulator of CpG methylation, we constructed stable UHRF1-knockdown HeLa cells using shRNA. We then performed cDNA microarray analysis and identified 28 genes up-regulated >2-fold in shUHRF1 HeLa cells compared to control cells expressing shCTL (Supplementary Table S5). Among these, *TXNIP* shows the largest increase in response to shUHRF1 HeLa cells (Fig. 1A).

We next utilised the Illumina Infinium MethylationEPIC method to perform whole-genome CpG methylation analysis in both cervical cancer and normal cervix tissue, as well as in cervical cancer cell lines (HeLa, SiHa, Caski). We found that among the common hypermethylated genes identified (Supplementary Tables S6 and S7, Supplementary Fig. S1), *TXNIP* showed the most significant levels of differential methylation in both cervical cancer tissue and cervical cancer cell lines compared to normal cervix tissue (Figs. 1B and 1C). These results suggest that *TXNIP* may be a down-stream target of UHRF1 in cervical cancer.

Expression of UHRF1 and TXNIP is inversely correlated in cervical cancer

To better understand the relationship between UHRF1 and TXNIP, their expression levels were measured in cervical cancer tissue and cervical cancer cell lines by western blotting. We found that UHRF1 was significantly increased in cervical cancer tissue (Fig. 2A) and cell lines (Fig. 2B) compared to respective controls. In contrast, TXNIP was decreased in cervical cancer compared to normal cervix tissue (Fig. 2A), as well as in cervical cancer lines versus control cell lines (Fig. 2B). Immunohistochemical staining for UHRF1 and TXNIP in normal cervix and cervical cancer tissue similarly showed increased expression of UHRF1 and decreased expression of TXNIP in cervical cancer tissue compared to normal cervix tissue (Figs. 2C and 2D), thereby confirming that expression levels of

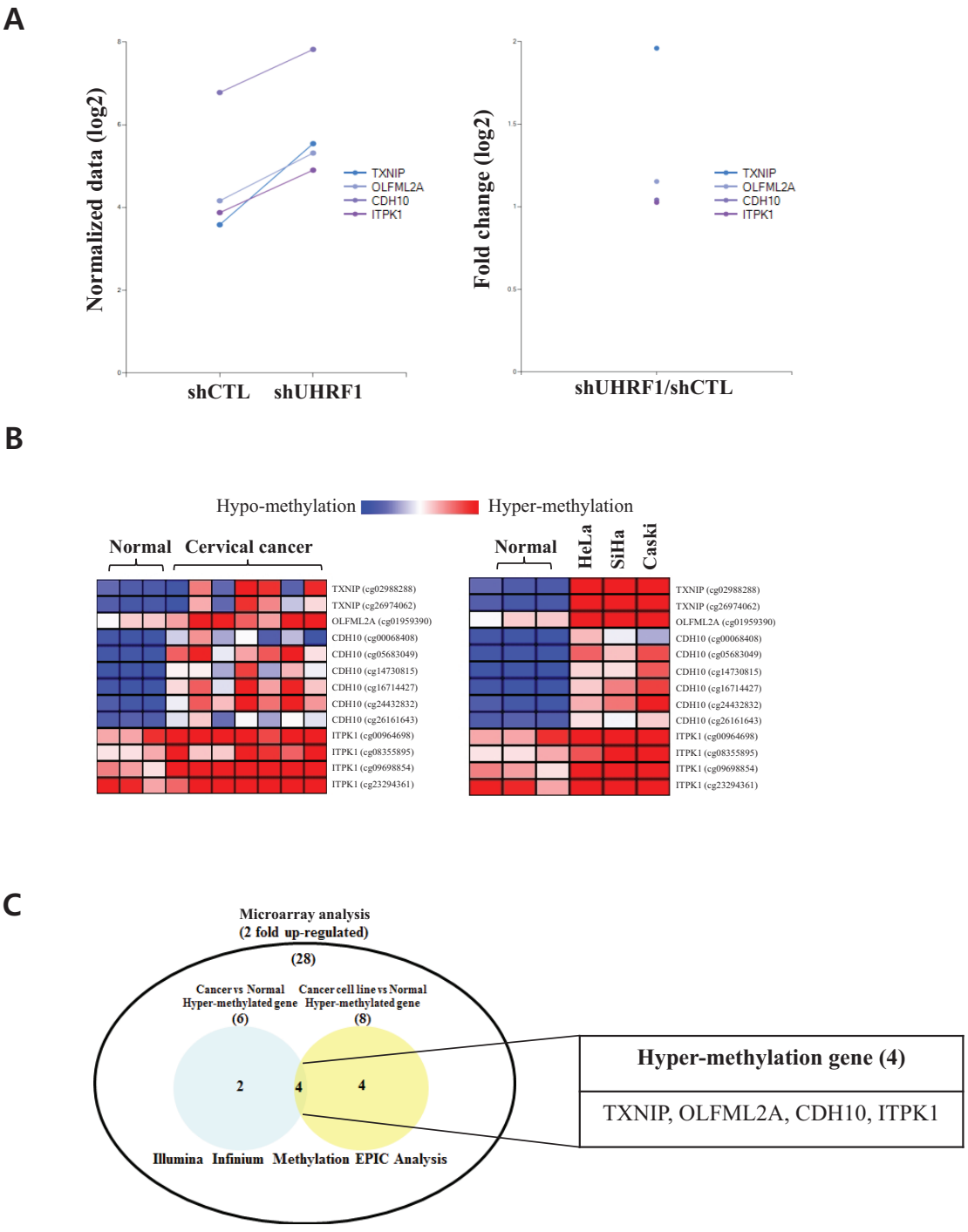

Fig. 1. *TXNIP* is highly induced in HeLa cells knocked down for expression of the epigenetic regulator UHRF1 and hypermethylated at CpG promoter regions in cervical cancer tissues and cell lines. (A) Normalised expression data (left) and fold-change in expression (right) of four genes highly induced by short hairpin (sh)RNA-mediated UHRF1 knockdown, as measured by cDNA microarray, plotted on a log2 scale. *TXNIP* is the most highly up-regulated gene in HeLa cells transfected with shRNA targeting UHRF1 (shUHRF1) compared to control shRNA (shCTL). (B) Heatmaps comparing the methylation status of the four up-regulated genes panel A. in normal tissue and cancer tissue or cancer cell lines, measured by whole-genome CpG methylation analysis. Left column shows that heatmap of hypermethylated genes in cervical cancer tissue (n = 7) tissues versus normal tissues (n = 3), and right column shows that heatmap of hypermethylated genes in cervical cancer cell lines (Caski, SiHa, and HeLa) versus normal tissues. DNA methylation values are represented using a colour scale from blue (low DNA methylation) to red (high DNA methylation). (C) Venn diagram showing the overlap of genes hypermethylated in both groups (Cancer tissues vs Normal tissues and Cervical cancer cell lines vs Normal tissues) that are also up-regulated >2-fold in UHRF1-knockdown cells. Four common hypermethylated genes were identified.

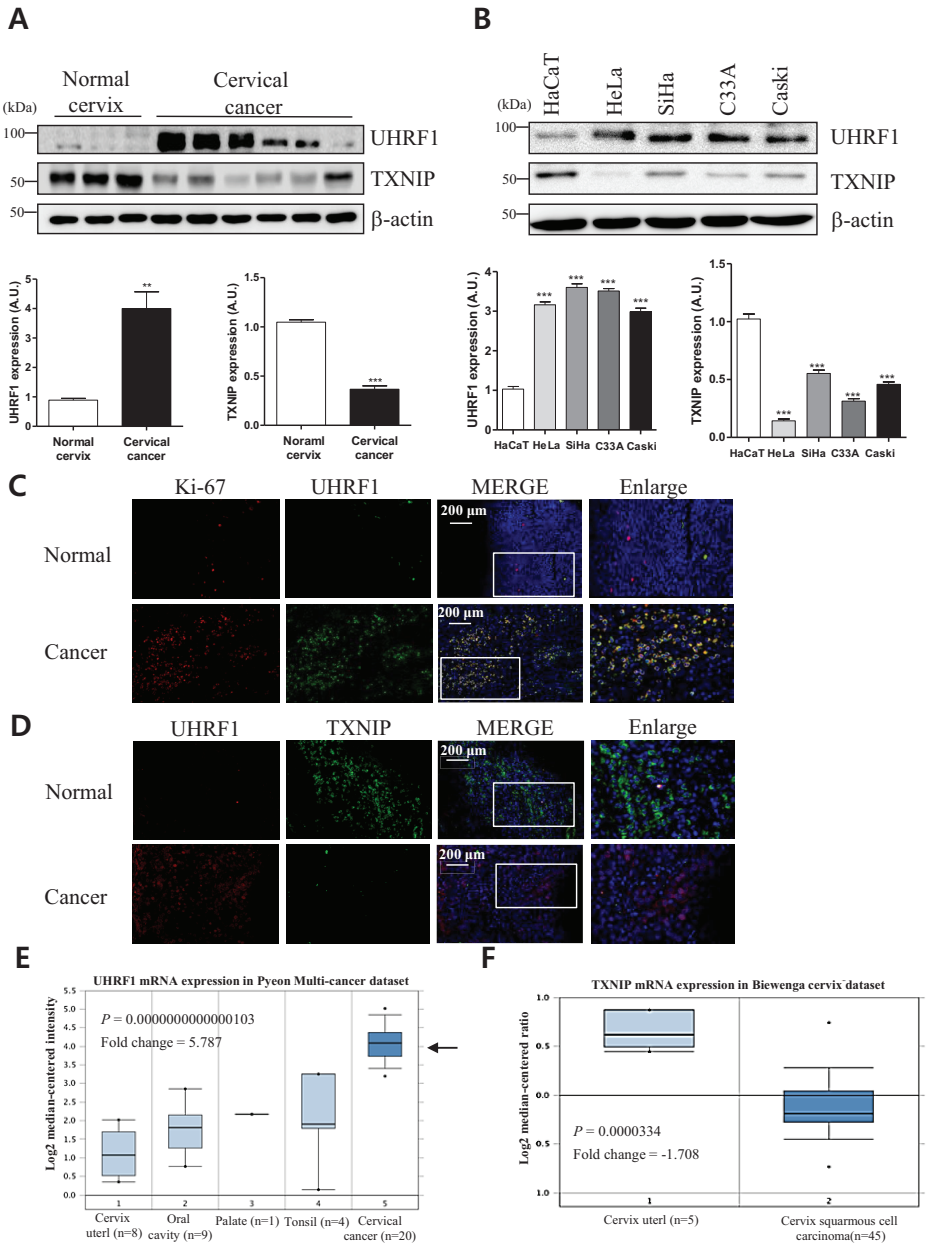

Fig. 2. Expression of UHRF1 and TXNIP in cervical cancer tissues and cell lines. Expression levels of UHRF1 and TXNIP were measured by western blot analysis in normal cervix tissues (n = 3) and cervical cancer (n = 22) (A) and in normal keratinocytes (HaCaT) and cervical cancer cell lines (HeLa, SiHa, C33A, Caski) (B). β-Actin was used as a control to ensure equivalent loading; band density values were normalised to β-actin and are graphed below. Data are presented as the mean ± SEM (n = 3). $^{**}P < 0.01$ and $^{***}P < 0.001$. Representative images of immunofluorescence staining for Ki-67 and UHRF1 (C) and for UHRF1 and TXNIP (D) in normal cervix and cervical cancer tissue. Scale bar = 200 μm. Oncomine database analysis of UHRF1 mRNA expression in the Pyeon multi-cancer dataset (Pyeon et al., 2007) that shows the significant higher expression of UHRF1 mRNA in cervical cancer indicated by arrow (E) and TXNIP mRNA expression in the Biewenga cervical cancer dataset (Biewenga et al., 2008) that shows the significant higher expression of TXNIP mRNA expression in cervical cancer (F).

these proteins were inversely correlated in cervical cancer. Additionally, we found that Ki-67 co-localised with UHRF1 in cervical cancer tissue, but not in the normal cervix (Figs. 2C and 2D).

We also analysed expression of UHRF1 and TXNIP in several datasets containing cervical cancer samples retrieved from the Oncomine database. Consistent with our expression data, we found that *UHRF1* mRNA was up-regulated in cervical cancer, whereas *TXNIP* mRNA was down-regulated compared to normal tissue (Figs. 2E and 2F), providing further evidence that expression of UHRF1 and TXNIP is inversely correlated in cervical cancer.

UHRF1 binds the *TXNIP* promoter and down-regulates TXNIP expression

UHRF1 binds at the inverted CCAAT domain in gene promoters and down-regulates expression by promoting methylation (Unoki et al., 2004). We therefore hypothesised that UHRF1 regulates *TXNIP* expression by binding to the inverted CCAAT domain in its promoter and inducing DNA methylation. To test this, we performed ChIP assays using anti-UHRF1 and negative control IgG antibodies in HeLa cells, with three pairs of primers specific to the region 1000 bp upstream of the *TXNIP* TSS (Figs. 3A and 3B, Supplementary Table S1). We detected UHRF1 binding in the region –780 to –491 bp upstream of the transcription start site (TSS), which contains an inverted CCAAT domain (Fig. 3C). We then compared

Fig. 3. UHRF1 binds to the inverted CCAAT (ATTGG) domain in the *TXNIP* promoter region and down-regulates expression of TXNIP. (A) Putative UHRF1-binding site in the *TXNIP* promoter and annealing sites for the three primer sets used in chromatin immunoprecipitation (ChIP) assays. (B) Arrows show the regions amplified by the three PCR primer sets, relative to the *TXNIP* gene. TSS, transcription start site. (C) Quantitative PCR (qPCR) analysis using the three different primer sets shown in panel A. of the DNA immunoprecipitated in ChIP assays with antibody against UHRF1 and negative control antibodies. (D) Fold-enrichment of UHRF1 at the *TXNIP* promoter measured by ChIP with anti-UHRF1 antibodies and qPCR with primer pair #2 in HeLa cells and two normal cell lines (HaCaT, ARPE-19). Expression of TXNIP measured by western blot analysis in HaCaT, ARPE-19, HeLa cells. Quantification of each band was normalised to the negative control.

UHRF1 binding to this region in HeLa cells versus two normal cell lines (HaCaT and ARPE-19). As expected, we measured higher UHRF1 binding and lower expression of TXNIP in HeLa cells compared to the other cell lines tested (Fig. 3D). These results suggest that UHRF1 binds to the inverted CCAAT domain in the *TXNIP* promoter and inhibits gene expression via

CpG methylation.

UHRF1 knockdown inhibits UHRF1 binding to *TXNIP* promoter and enhances TXNIP expression through promoter demethylation

We next measured UHRF1 binding to the *TXNIP* promoter in HeLa cells stably expressing shUHRF1 and shCTL and found that shRNA-mediated UHRF1 silencing decreased UHRF1 binding to the *TXNIP* promoter and increased TXNIP expression (Fig. 4A). Using pyrosequencing, we then analysed *TXNIP* promoter methylation in shCTL and UHRF1-knockdown HeLa cells, revealing increased methylation at the CpG site located −780 to −491 bp upstream of the *TXNIP* TSS in shCTL versus shUHRF1 cells (Fig. 4B). We also designed primer sets specific for methylated or unmethylated *TXNIP* promoter and performed MSP on shUHRF1 and shCTL cells. Consistent with pyrosequencing data, the methylated DNA-specific product was increased in shCTL cells relative to shUHRF1 cells, whereas the band specific for unmethylated DNA was increased in shUHRF1 HeLa cells (Fig. 4C). We further tested the effect of the DNA methylation inhibitor 5azadC on *TXNIP* promoter methylation status in HeLa cells and found that treatment with 5azadC decreased levels of methylated *TXNIP* (Fig. 4D). We then measured TXNIP expression in HeLa cells co-treated with 5azadC and TSA, a known histone deacetylase (HDAC) inhibitor, and found that TXNIP levels were significantly increased in HeLa cells after 5azadC and TSA co-treatment (Fig. 4E). Collectively, these data indicate shRNA-mediated UHRF1 knockdown decreases binding at the *TXNIP* promoter, resulting in decreased *TXNIP* promoter methylation and increased TXNIP expression.

The TXNIP promoter is highly methylated in human cervical cancer

We further used pyrosequencing analysis to measure levels of CpG methylation at the *TXNIP* promoter in cervical cancer samples compared to normal cervix tissue. We detected increased methylation in early-stage cancer relative to healthy controls, although the difference was not statistically significant (Fig. 4F). Notably, however, levels of *TXNIP* promoter CpG methylation were found to be significantly increased in advanced-stage cervical cancer compared to normal cervix tissue (Fig. 4F). MSP analysis further showed increased hypermethylation in cervical cancer relative to normal cervix tissue (Fig. 4G). These data therefore demonstrate that the *TXNIP* promoter is highly methylated in cervical cancer, particularly in late-state disease.

TXNIP protein induced by UHRF1 knockdown translocates to the nucleus and regulates apoptosis through cell cycle arrest in HeLa cells

UHRF1 is involved in regulation of the cell cycle and apoptosis (Zhang et al., 2018). Therefore, we measured the effect of stable UHRF1 knockdown on these cellular processes in HeLa cells. We first confirmed that TXNIP expression was significantly decreased in shUHRF1-expressing HeLa cells compared to shCTL cells (Fig. 5A). To further validate these results, we also measured TXNIP expression in HeLa cells transfected with small interfering (si)RNA targeting UHRF1 or control siRNA. As expected, we detected increased TXNIP expression in UHRF1-knockdown cells compared to control cells (Supplementary Fig. S2). We then measured cellular localisation of UHRF1 and TXNIP in fractionated cells and found that UHRF1 was primarily in the nuclear fraction, whereas TXNIP was localised in both the cytosol and nucleus (Fig. 5B). As expected, in UHRF1-knockdown cells, nuclear UHRF1 expression was decreased, and TXNIP expression increased in both the nuclear and cytosol fractions. Immunocytochemistry also showed that significantly nuclear UHRF1 expression was decreased and TXNIP expression increased in both the nuclear and cytosol of UHRF1-knockdown cells (Figs. 5C and 5D).

Trx1, a negative regulator of TXNIP, is involved in cellular redox balance and cell cycle control in cancer and is regulated by UHRF1. We therefore examined whether UHRF1 causes cell cycle arrest through modulation of Thioredoxin (expression. We detected decreased expression of Trx1 and increased p27 expression in shUHRF1-expressing HeLa cells by western blot analysis (Fig. 5E), suggesting UHRF1 knockdown induces cell cycle arrest by increasing expression of TXNIP through p27. We then performed TUNEL assays to measure apoptosis and found that TUNEL-positive cells were increased by 32% in UHRF1-knockdown cells compared to controls. These results suggest that TXNIP induces cell death through UHRF1 (Fig. 5F).

UHRF1 antagonist thymoquinone induces apoptosis and cell cycle arrest in HeLa cells

To further confirm that UHRF1 regulates TXNIP, we treated HeLa cells with various concentrations of a highly selective UHRF1 antagonist, thymoquinone (TQ), and determined cell viability using MTT assays. From these experiments, the half-maximal inhibitory concentration (IC_{50}) value of TQ for HeLa cells was estimated to be 30 μM (Fig. 6A). We then measured TXNIP expression in TQ-treated HeLa cells and found that treatment strongly enhanced the levels of TXNIP expression (Fig. 6B).

We next measured apoptosis in HeLa cells treated with 30 μM TQ for 24 h by FACS analysis and TUNEL staining. We found that apoptotic cells, in the $SubG_1$ phase, were increased 32% in TQ-treated cells compared to controls (Fig. 6C). The number of TUNEL-positive cells also increased by 28% in response to TQ treatment compared to no-treatment control (Fig. 6D). Consistent with these results, western blot analysis showed that similar to UHRF1 knockdown, TQ treatment significantly reduced levels of Trx1 and increases p27 expression compared to untreated cells (Fig. 6E). Additionally, we observed significantly increased levels of cleaved PARP, a marker for apoptosis, in TQ-treated HeLa cells versus no-treatment control (Fig. 6F). Thus, our data indicate that TXNIP induces cell death through cell cycle arrest by UHRF1 inhibition.

HPV E6/E7 induces UHRF1 expression through USP7

USP7 regulates stability of UHRF1, thereby maintaining DNA methylation, and its expression is induced by viral proteins (Beck et al., 2018; Felle et al., 2011). Therefore, we tested whether HPV promotes USP7 expression and if HPV-induced USP7 can regulate TXNIP expression through up-regulation

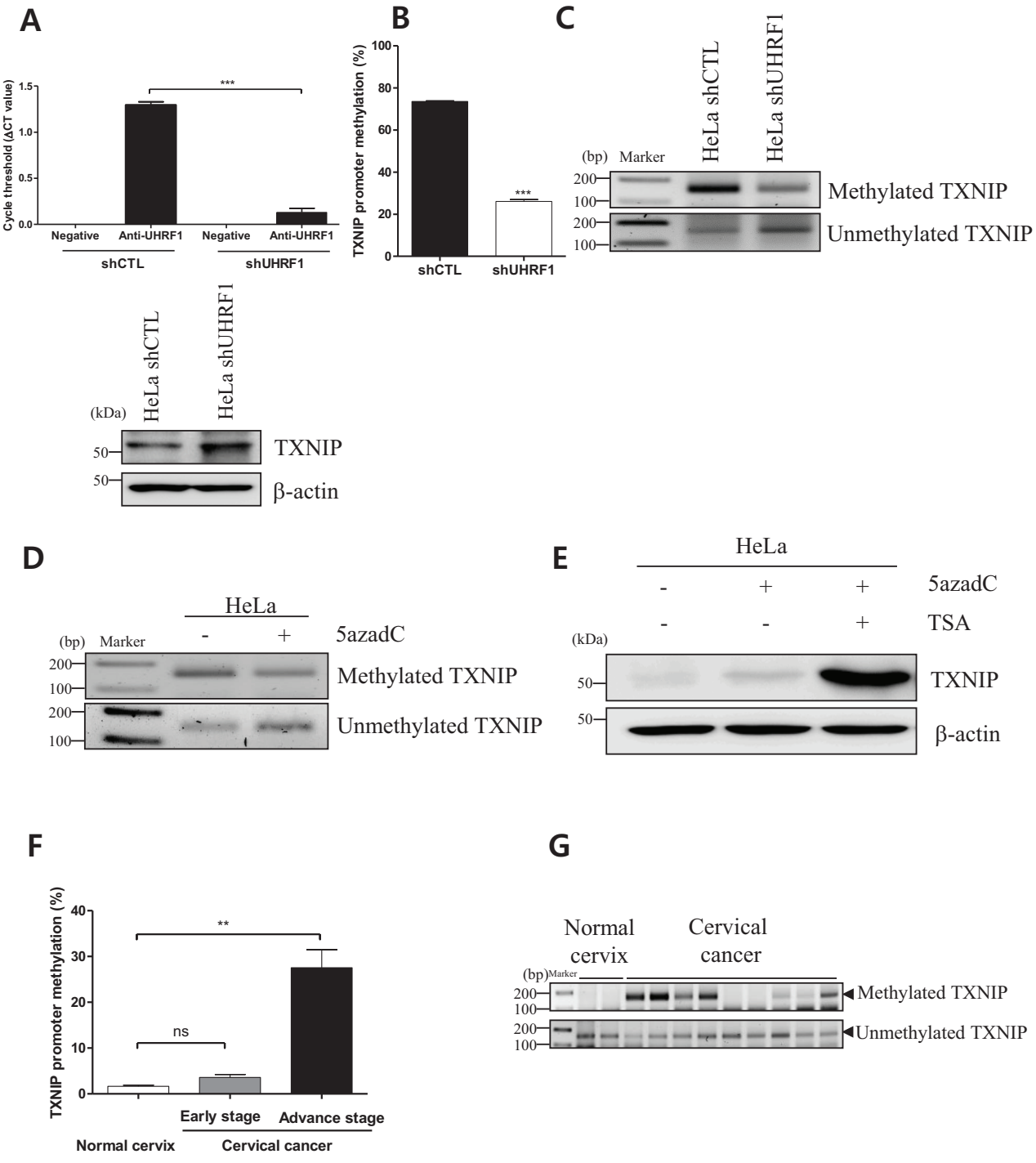

Fig. 4. UHRF1 knockdown enhances demethylation of *TXNIP* promoter region and *TXNIP* promoter region is hypermethylated in cervical cancer. (A) Absolute ΔCT value of UHRF1 at the *TXNIP* promoter measured by ChIP with anti-UHRF1 antibodies and qPCR analyses using primer set #2 in shUHRF1 and shCTL HeLa cells. Expression of TXNIP measured by western blot analysis in shUHRF1 HeLa and shCTL HeLa cells. (B) Pyrosequencing of the *TXNIP* promoter region in shUHRF1 HeLa cells compared to shCTL cells. (C) Methylation status of the *TXNIP* promoter region as determined by MSP in shUHRF1 and shCTL HeLa cells. (D) MSP performed on HeLa cells treated with 10 μM 5-aza-deoxycytidine (5azadC) for 24 h and untreated control cells. (E) HeLa cells were incubated with 10 μM 5azadC with and without 1 μM Trichostatin A (TSA) for 24 h, and TXNIP expression was determined by western blot analysis. β-Actin was used as a control to ensure equivalent loading. (F) Pyrosequencing of the *TXNIP* promoter region in early-stage (n = 14) and advanced-stage (n = 8) cervical cancer tissues compared to normal tissues (n = 3). (G) Methylation status of the *TXNIP* promoter region as determined by MSP in cervical cancer tissues (n = 22) compared to normal cervix tissues (n = 2). ns, not significant. $^{**}P < 0.01$, $^{***}P < 0.001$.

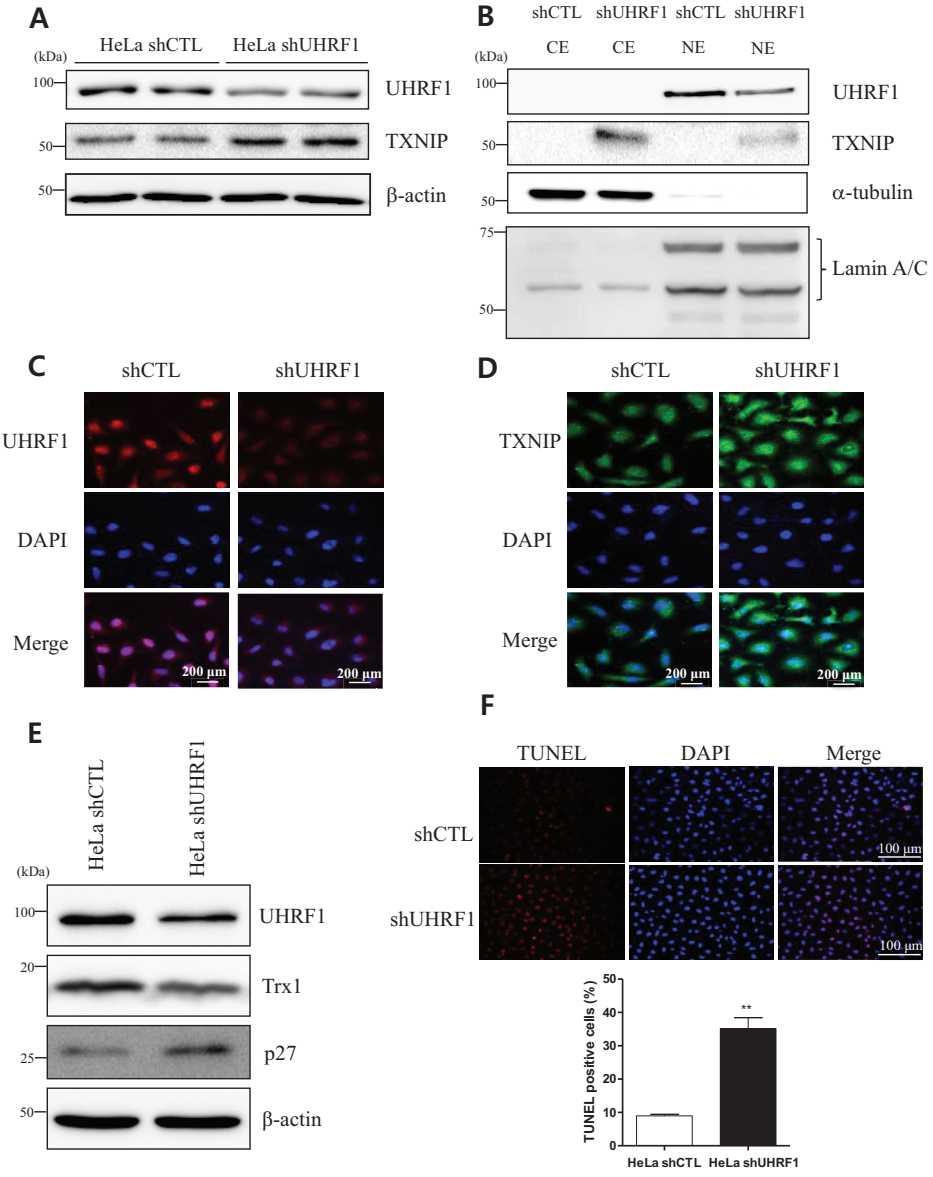

Fig. 5. UHRF1-knockdown-induced TXNIP translocates to the nucleus and regulates apoptosis in HeLa cells. (A) Expression of UHRF1 and TXNIP measured by western blot analysis in shUHRF1 and shCTL HeLa cells. β-Actin was used as a control to ensure equivalent loading. (B) Western blot analysis for UHRF1 and TXNIP expression in cellular fractions from shCTL and shUHRF1 HeLa cells. Equal amounts of protein (20 μg) from each fraction were analysed by immunoblotting, with blots stained for α-tubulin, as a cytoplasmic marker, and lamin A/C, as a nuclear marker. CE, cytosolic elution; NE, nuclear elution. Representative images of immunofluorescence staining for (C) UHRF1 (red) and (D) TXNIP (green) in shUHRF1 and shCTL HeLa cells. DAPI nuclear staining is shown in blue. (E) Western blot analysis to measure expression of UHRF1, the reactive oxygen species (ROS) scavenger-related Trx1, and cell cycle-associated p27 in shCTL and shUHRF1 HeLa cells. β-Actin was used as a control to ensure equivalent loading. (F) Representative images of TUNEL staining in shUHRF1 and shCTL HeLa cells. DAPI nuclear staining is shown in blue. The graph indicates quantification of TUNEL-positive cell staining. Data are presented as the mean ± SEM from three independent experiments (**P < 0.01).

of UHRF1. Western blot analysis revealed that expression of USP7 was indeed increased in cervical cancer tissues compared to normal cervix (Fig. 7A). We then used the online tool GEO2R to analyse USP7 expression in cervical cancer and normal cervix samples from existing datasets and found that expression of USP7 was increased in cervical cancer compared to normal cervix (Fig. 7B).

To directly test the effect of HPV protein expression on USP7, we overexpressed HPV16 E6/E7 in two normal cell lines (HaCaT, ARPE-19). We found that expression of USP7, DNMT1, and UHRF1 was increased in HPV16 E6/E7-overexpressing cells, whereas TXNIP expression was decreased (Figs. 7C and 7D). This suggests that the vial protein stabilises DNMT1 and UHRF1 via USP7, thereby increasing methylation activity and decreasing TXNIP expression. We further measured expression of these proteins in HEK001 cells, which over-express HPV16 E6/E7, transfected with siRNA targeting E6/E7 (siE6/E7). As predicted, we detected decreased expression of USP7, UHRF1, and DNMT1, and increased TXNIP expression in siE6/E7-transfected cells relative to controls (Fig. 7E). Collectively, these data indicate that HPV E6/E7 induces expression of USP7, which promotes TXNIP methylation through the epigenetic regulator UHRF1, leading to enhanced cell proliferation and decreased apoptosis in cervical cancer (Fig. 7F).

DISCUSSION

In this study, we show that UHRF1 down-regulated *TXNIP* expression in cervical cancer by promoting hypermethylation at the *TXNIP* promoter, thereby contributing to UHRF1-mediated carcinogenesis. UHRF1 is involved in maintaining DNA methylation, and overexpression of UHRF1 induces oncogenesis through DNA methylation and down-regulation of

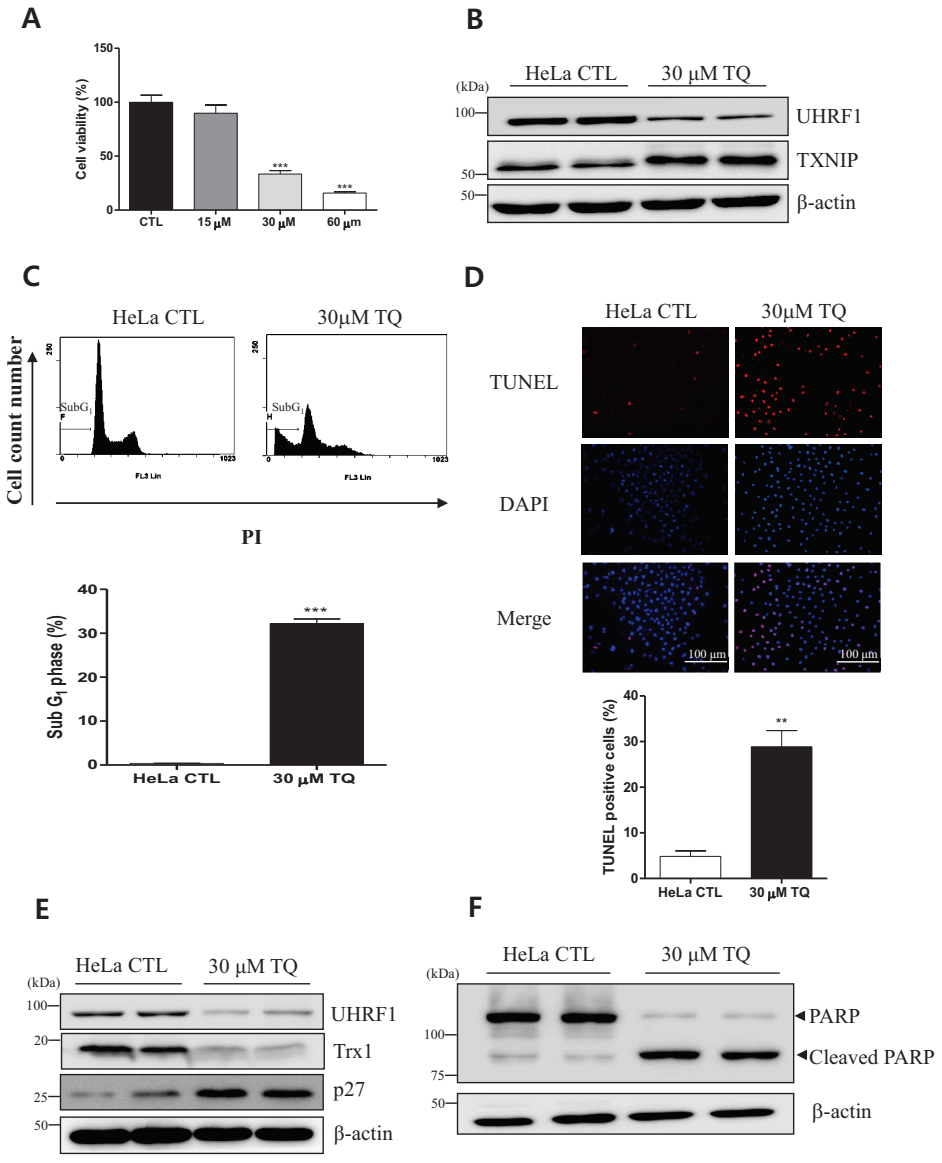

Fig. 6. The UHRF1 antagonist, thymoquinone (TQ), induces apoptosis and cell cycle arrest in HeLa cells. (A) HeLa cells were treated with different concentrations of TQ (15 μM, 30 μM, 60 μM) for 24 h, and cell metabolic activity was measured using the MTT assay to determine the rate of HeLa cell death in response to TQ treatment. Percent cell survival is presented as the mean ± SEM (n = 16). ***P < 0.001 compared to control (CTL). (B) Expression of UHRF1 and TXNIP measured by western blot analysis in HeLa cells treated 30 μM TQ for 24 h and the untreated CTL. (C) HeLa cells (1×10^5 cells/ml) were treated with 30 μM TQ for 24 h. Cells were then fixed, stained with PI, and analysed by flow cytometry. Bar diagram indicates the percentage of cells in the Sub-G_1 phase of the cell cycle. Data are presented as the mean ± SEM (n = 3). ***P < 0.001, compared to untreated control. (D) HeLa cells were treated with 30 μM TQ for 24 h and analysed by TUNEL staining. Percentages of TUNEL-positive cells are presented as mean ± SEM (n = 3). **P < 0.01, compared to untreated control. Western blot analysis to measure expression of UHRF1, p27, and Trx1 (E) and PARP and cleaved PARP (F) in HeLa cells treated with 30 μM TQ for 24 h and untreated CTL. β-Actin was used as a control to ensure equivalent loading.

TSGs in numerous types of cancer, including cervical cancer (Alhosin et al., 2011; Babbio et al., 2012; Ge et al., 2016; Unoki et al., 2009). A previous study reported that UHRF1 is up-regulated by the HPV oncogenic E6/E7 proteins and, in turn, down-regulates UbcH8 expression to inhibit apoptosis in cervical cancer (Zhang et al., 2018). However, despite these findings, the function and down-stream targets of UHRF1 in cervical cancer remain unclear. Here, we constructed a stable UHRF1-knockdown HeLa cell line and performed cDNA microarray analysis. From this analysis, we identified TXNIP as a novel down-stream target of UHRF1. We then performed whole-genome methylation profiling to identify genes that are hypermethylated in both cervical cancer tissues and cervical cancer cell lines compared to normal cervix tissue (Supplementary Tables S6 and S7, respectively). Among these genes, *TXNIP* was identified as the most highly differentially hypermethylated gene in cervical cancer tissue and cell lines compared to normal controls.

TXNIP is classified as a TSG, and accordingly, its expression is decreased in many cancer types (Baldan et al., 2015; Morrison et al., 2014; Nie et al., 2015). Recently, it was reported that UHRF1 regulates TXNIP expression through DNA methylation in RCC (Jiao et al., 2019). Therefore, we hypothesised that UHRF1-induced methylation may similarly modulate TXNIP to induce cervical carcinogenesis. Here, we detected elevated expression of UHRF1 and decreased TXNIP expression in cervical cancer tissue compared to normal cervix by both western blot and immunohistochemistry, indicating an inverse correlation between expression of these proteins. A similar expression pattern was also detected in datasets from the Oncomine database, providing additional evidence that TXNIP is negatively regulated by UHRF1.

Using ChIP analysis, we further identified the UHRF1-binding site in a region −780 to −479 bp upstream of the *TXNIP* TSS. Notably, this region contains an inverted CCAAT domain —the known UHRF1-binding motif (Unoki et al., 2004). Jiao

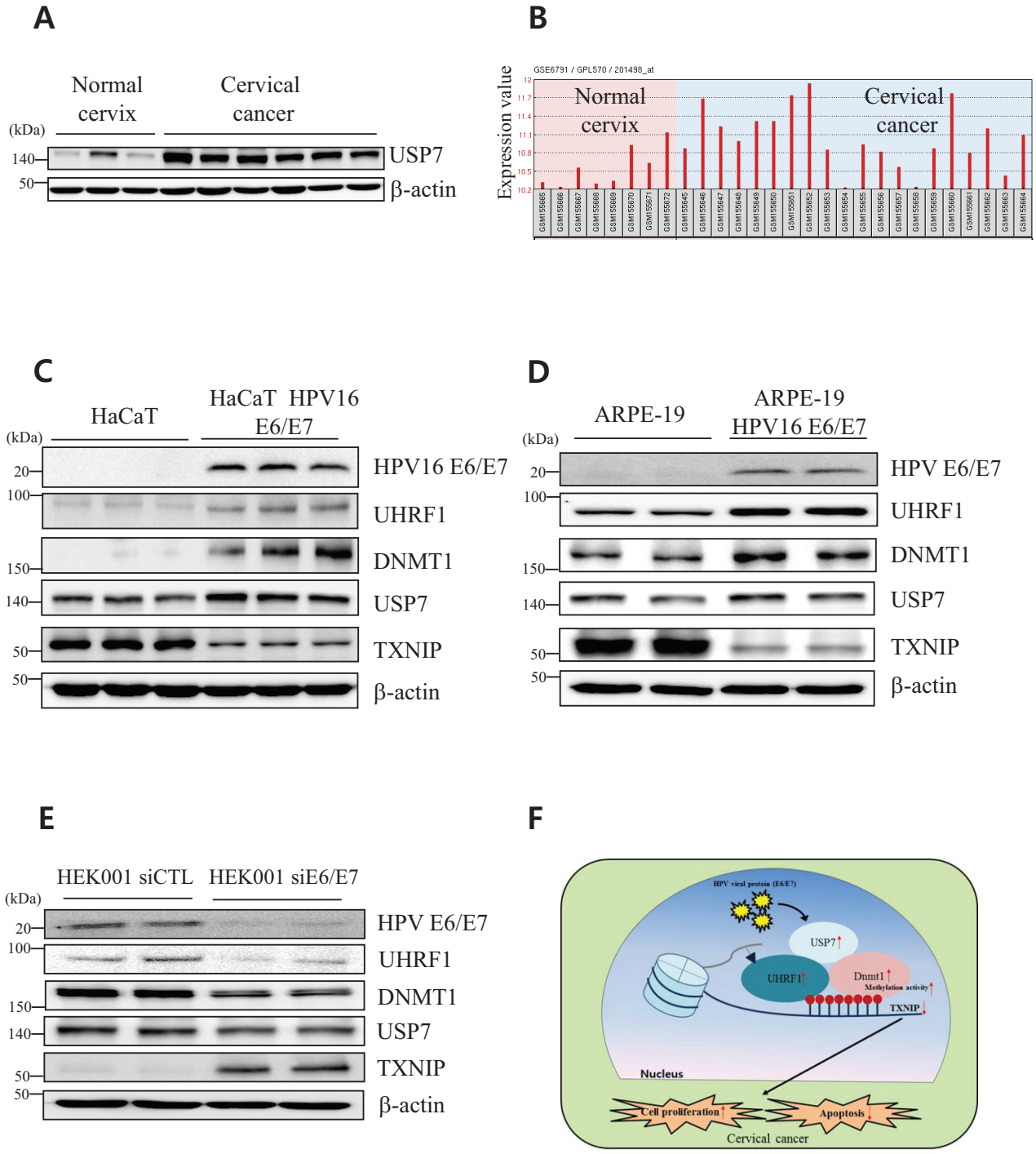

Fig. 7. HPV E6/E7 induces UHRF1 expression through USP7. (A) Expression of USP7 measured by western blot in cervical cancer tissue (n = 22) and normal cervix tissue (n = 3). β-Actin was used as a control to ensure equivalent loading. (B) Relative expression levels of *USP7* in cervical cancer tissue (n = 20) and normal cervical tissue (n = 8) samples from the NCBI Gene Expression Omnibus (GEO2R). GSE6791 samples were analysed with the Affymetrix HumanGenome U133 Plus 2.0 Array (GPL570). Western blot analysis to measure expression of HPV E6/E7, UHRF1, DNMT1, USP7, and TXNIP in HaCaT cells transfected with the HPV16 E6/E7 overexpression plasmid and control plasmid transfected HaCaT cells (C), ARPE-19 cells transfected with the HPV16 E6/E7 overexpression plasmid and control plasmid transfected ARPE-19 cells (D), and HEK001 cells transfected with siRNA against E6/E7 (HEK001siE6/E7) or scramble siRNA (siCTL) (E), β-actin was used as a control to ensure equivalent loading. (F) Schematic model of the proposed mechanism for HPV E6/E7-mediated epigenetic regulation of TXNIP by UHRF1. HPV E6/E7 induces expression of USP7, which promotes hypermethylation of TXNIP through the action of the epigenetic regulator, UHRF1. This down-regulation of TXNIP enhances cell proliferation and decreases apoptosis in cervical cancer.

et al. (2019) previously reported UHRF1-binding domains in the *TXNIP* promoter in regions −945 to −826 bp and −610 to −329 bp upstream of the TSS; however, they did not detect inverted CCAAT domains in these regions. Here, we also performed pyrosequencing and MSP in UHRF1-knockdown and shCTL cells, as well as in cervical cancer and normal tissue, which clearly show that UHRF1 induces hypermethylation in the CpG island of the *TXNIP* promoter region. Interestingly, a negative correlation between TXNIP expression and patient clinicopathological features, such as tumour differentiation status, was observed in RCC (Jiao et al., 2019), suggesting TXNIP expression may have similar prognostic value in cervical cancer.

We further found that down-regulation of UHRF1 by shRNA or treatment with UHRF1 antagonist, TQ, increased TXNIP expression, induced cell cycle arrest, and increased levels of apoptosis, further suggesting that epigenetic modification of TXNIP by UHRF1 is involved in cervical carcinogenesis. It has been shown that expression of USP7, which regulates stability of UHRF1 for maintaining DNA methylation, is induced by proteins from numerous viruses (Felle et al., 2011). Thus, we predicted that the HPV E6/E7 oncoproteins might induce expression of USP7, which in turn, promotes UHRF1 activity and consequently, down-regulates TXNIP expression. Indeed, we found that HPV E6/E7 induced USP7 in cervical cancer, leading to hypermethylated *TXNIP* through the action of the epigenetic regulator UHRF1, consistent with previous findings (Jiao et al., 2019).

In summary, we propose a model whereby HPV E6/E7 oncoproteins induce cell proliferation and decreased apoptosis through UHRF1-mediated *TXNIP* promoter methylation and down-regulation of TXNIP expression in cervical cancer (Fig. 7F). These data suggest that TXNIP could represent a possible therapeutic target for cervical cancer, as well as other types of virus-related cancer.

Note: Supplementary information is available on the Molecules and Cells website (www.molcells.org).

ACKNOWLEDGMENTS

This research was supported by National Research Foundation of Korea (NRF-2015R1A5A2008833 and NRF-2019R1F1A1058581) and Ministry of Agriculture, Food and Rural Affairs (117082-03).

AUTHOR CONTRIBUTIONS

M.J.K. and W.S.C. designed and wrote the manuscript. M.J.K. performed the experiments. H.J.L, M.Y.C., Y.S.K., and S.S.K. gave technical support and conceptual advice. J.K.S. interpreted the data. W.S.C. and Y.S.K. edited the manuscript. All authors participated in review of the manuscript.

CONFLICT OF INTEREST

The authors have no potential conflicts of interest to disclose.

ORCID

Min Jun Kim https://orcid.org/0000-0002-9262-2039
Han Ju Lee https://orcid.org/0000-0002-7043-0191
Mee Young Choi https://orcid.org/0000-0002-1474-0443
Sang Soo Kang https://orcid.org/0000-0001-9424-2067
Yoon Sook Kim https://orcid.org/0000-0002-6485-5265
Jeong Kyu Shin https://orcid.org/0000-0001-9050-0874
Wan Sung Choi https://orcid.org/0000-0001-9508-6764

REFERENCES

Alhosin, M., Sharif, T., Mousli, M., Etienne-Selloum, N., Fuhrmann, G., Schini-Kerth, V.B., and Bronner, C. (2011). Down-regulation of UHRF1, associated with re-expression of tumor suppressor genes, is a common feature of natural compounds exhibiting anti-cancer properties. J. Exp. Clin. Cancer Res. *30*, 41.

Babbio, F., Pistore, C., Curti, L., Castiglioni, I., Kunderfranco, P., Brino, L., Oudet, P., Seiler, R., Thalman, G.N., Roggero, E., et al. (2012). The SRA protein UHRF1 promotes epigenetic crosstalks and is involved in prostate cancer progression. Oncogene *31*, 4878-4887.

Baldan, F., Mio, C., Lavarone, E., Di Loreto, C., Puglisi, F., Damante, G., and Puppin, C. (2015). Epigenetic bivalent marking is permissive to the synergy of HDAC and PARP inhibitors on TXNIP expression in breast cancer cells. Oncol. Rep. *33*, 2199-2206.

Barrett, T., Wilhite, S.E., Ledoux, P., Evangelista, C., Kim, I.F., Tomashevsky, M., Marshall, K.A., Phillippy, K.H., Sherman, P.M., Holko, M., et al. (2013). NCBI GEO: archive for functional genomics data sets--update. Nucleic Acids Res. *41*, D991-D995.

Beck, A., Trippel, F., Wagner, A., Joppien, S., Felle, M., Vokuhl, C., Schwarzmayr, T., Strom, T.M., von Schweinitz, D., Langst, G., et al. (2018). Overexpression of UHRF1 promotes silencing of tumor suppressor genes and predicts outcome in hepatoblastoma. Clin. Epigenetics *10*, 27.

Biewenga, P., Buist, M.R., Moerland, P.D., Ver Loren van Themaat, E., van Kampen, A.H., ten Kate, F.J., and Baas, F. (2008). Gene expression in early stage cervical cancer. Gynecol. Oncol. *108*, 520-526.

Bostick, M., Kim, J.K., Esteve, P.O., Clark, A., Pradhan, S., and Jacobsen, S.E. (2007). UHRF1 plays a role in maintaining DNA methylation in mammalian cells. Science *317*, 1760-1764.

Dunn, L.L., Buckle, A.M., Cooke, J.P., and Ng, M.K. (2010). The emerging role of the thioredoxin system in angiogenesis. Arterioscler. Thromb. Vasc. Biol. *30*, 2089-2098.

Dutta, K.K., Nishinaka, Y., Masutani, H., Akatsuka, S., Aung, T.T., Shirase, T., Lee, W.H., Yamada, Y., Hiai, H., Yodoi, J., et al. (2005). Two distinct mechanisms for loss of thioredoxin-binding protein-2 in oxidative stress-induced renal carcinogenesis. Lab. Invest. *85*, 798-807.

El-Araby, A.M., Fouad, A.A., Hanbal, A.M., Abdelwahab, S.M., Qassem, O.M., and El-Araby, M.E. (2016). Epigenetic pathways of oncogenic viruses: therapeutic promises. Arch. Pharm. (Weinheim) *349*, 73-90.

Elgort, M.G., O'Shea, J.M., Jiang, Y., and Ayer, D.E. (2010). Transcriptional and translational downregulation of thioredoxin interacting protein is required for metabolic reprogramming during G(1). Genes Cancer *1*, 893-907.

Erkeland, S.J., Palande, K.K., Valkhof, M., Gits, J., Danen-van Oorschot, A., and Touw, I.P. (2009). The gene encoding thioredoxin-interacting protein (TXNIP) is a frequent virus integration site in virus-induced mouse leukemia and is overexpressed in a subset of AML patients. Leuk. Res. *33*, 1367-1371.

Esteller, M. (2008). Epigenetics in cancer. N. Engl. J. Med. *358*, 1148-1159.

Felle, M., Joppien, S., Nemeth, A., Diermeier, S., Thalhammer, V., Dobner, T., Kremmer, E., Kappler, R., and Langst, G. (2011). The USP7/Dnmt1 complex stimulates the DNA methylation activity of Dnmt1 and regulates the stability of UHRF1. Nucleic Acids Res. *39*, 8355-8365.

Ge, T.T., Yang, M., Chen, Z., Lou, G., and Gu, T. (2016). UHRF1 gene silencing inhibits cell proliferation and promotes cell apoptosis in human cervical squamous cell carcinoma CaSki cells. J. Ovarian Res. *9*, 42.

Gronbaek, K., Hother, C., and Jones, P.A. (2007). Epigenetic changes in cancer. APMIS *115*, 1039-1059.

Han, S.H., Jeon, J.H., Ju, H.R., Jung, U., Kim, K.Y., Yoo, H.S., Lee, Y.H., Song, K.S., Hwang, H.M., Na, Y.S., et al. (2003). VDUP1 upregulated by TGF-beta1 and 1,25-dihydorxyvitamin D3 inhibits tumor cell growth by blocking cell-cycle progression. Oncogene *22*, 4035-4046.

Hong, K., Xu, G., Grayson, T.B., and Shalev, A. (2016). Cytokines regulate beta-cell thioredoxin-interacting protein (TXNIP) via distinct mechanisms and pathways. J. Biol. Chem. *291*, 8428-8439.

Jeon, J.H., Lee, K.N., Hwang, C.Y., Kwon, K.S., You, K.H., and Choi, I. (2005). Tumor suppressor VDUP1 increases p27(kip1) stability by inhibiting JAB1. Cancer Res. *65*, 4485-4489.

Jiao, D., Huan, Y., Zheng, J., Wei, M., Zheng, G., Han, D., Wu, J., Xi, W., Wei, F., Yang, A.G., et al. (2019). UHRF1 promotes renal cell carcinoma progression through epigenetic regulation of TXNIP. Oncogene *38*, 5686-5699.

Kaimul, A.M., Nakamura, H., Masutani, H., and Yodoi, J. (2007). Thioredoxin and thioredoxin-binding protein-2 in cancer and metabolic syndrome. Free Radic. Biol. Med. *43*, 861-868.

Lindner, H.A. (2007). Deubiquitination in virus infection. Virology *362*, 245-256.

Liu, Y. and Min, W. (2002). Thioredoxin promotes ASK1 ubiquitination and degradation to inhibit ASK1-mediated apoptosis in a redox activity-independent manner. Circ. Res. *90*, 1259-1266.

Morrison, J.A., Pike, L.A., Sams, S.B., Sharma, V., Zhou, Q., Severson, J.J., Tan, A.C., Wood, W.M., and Haugen, B.R. (2014). Thioredoxin interacting protein (TXNIP) is a novel tumor suppressor in thyroid cancer. Mol. Cancer *13*, 62.

Nie, W., Huang, W., Zhang, W., Xu, J., Song, W., Wang, Y., Zhu, A., Luo, J., Huang, G., Wang, Y., et al. (2015). TXNIP interaction with the Her-1/2 pathway contributes to overall survival in breast cancer. Oncotarget *6*, 3003-3012.

Poreba, E., Broniarczyk, J.K., and Gozdzicka-Jozefiak, A. (2011). Epigenetic mechanisms in virus-induced tumorigenesis. Clin. Epigenetics *2*, 233-247.

Pyeon, D., Newton, M.A., Lambert, P.F., den Boon, J.A., Sengupta, S., Marsit, C.J., Woodworth, C.D., Connor, J.P., Haugen, T.H., Smith, E.M., et al. (2007). Fundamental differences in cell cycle deregulation in human papillomavirus-positive and human papillomavirus-negative head/neck and cervical cancers. Cancer Res. *67*, 4605-4619.

Rhodes, D.R., Yu, J., Shanker, K., Deshpande, N., Varambally, R., Ghosh, D., Barrette, T., Pandey, A., and Chinnaiyan, A.M. (2004). ONCOMINE: a cancer microarray database and integrated data-mining platform. Neoplasia *6*, 1-6.

Saitoh, M., Nishitoh, H., Fujii, M., Takeda, K., Tobiume, K., Sawada, Y., Kawabata, M., Miyazono, K., and Ichijo, H. (1998). Mammalian thioredoxin is a direct inhibitor of apoptosis signal-regulating kinase (ASK) 1. EMBO J. *17*, 2596-2606.

Sharif, J., Muto, M., Takebayashi, S., Suetake, I., Iwamatsu, A., Endo, T.A., Shinga, J., Mizutani-Koseki, Y., Toyoda, T., Okamura, K., et al. (2007). The SRA protein Np95 mediates epigenetic inheritance by recruiting Dnmt1 to methylated DNA. Nature *450*, 908-912.

Sheng, Y., Wang, H., Liu, D., Zhang, C., Deng, Y., Yang, F., Zhang, T., and Zhang, C. (2016). Methylation of tumor suppressor gene CDH13 and SHP1 promoters and their epigenetic regulation by the UHRF1/PRMT5 complex in endometrial carcinoma. Gynecol. Oncol. *140*, 145-151.

Unoki, M., Kelly, J.D., Neal, D.E., Ponder, B.A., Nakamura, Y., and Hamamoto, R. (2009). UHRF1 is a novel molecular marker for diagnosis and the prognosis of bladder cancer. Br. J. Cancer *101*, 98-105.

Unoki, M., Nishidate, T., and Nakamura, Y. (2004). ICBP90, an E2F-1 target, recruits HDAC1 and binds to methyl-CpG through its SRA domain. Oncogene *23*, 7601-7610.

Wan, X., Yang, S., Huang, W., Wu, D., Chen, H., Wu, M., Li, J., Li, T., and Li, Y. (2016). UHRF1 overexpression is involved in cell proliferation and biochemical recurrence in prostate cancer after radical prostatectomy. J. Exp. Clin. Cancer Res. *35*, 34.

Wei, M., Jiao, D., Han, D., Wu, J., Wei, F., Zheng, G., Guo, Z., Xi, W., Yang, F., Xie, P., et al. (2017). Knockdown of RNF2 induces cell cycle arrest and apoptosis in prostate cancer cells through the upregulation of TXNIP. Oncotarget *8*, 5323-5338.

Welsh, S.J., Bellamy, W.T., Briehl, M.M., and Powis, G. (2002). The redox protein thioredoxin-1 (Trx-1) increases hypoxia-inducible factor 1alpha protein expression: Trx-1 overexpression results in increased vascular endothelial growth factor production and enhanced tumor angiogenesis. Cancer Res. *62*, 5089-5095.

Yu, Q. (2008). Cancer gene silencing without DNA hypermethylation. Epigenetics *3*, 315-317.

Zhang, Q., Qiao, L., Wang, X., Ding, C., and Chen, J.J. (2018). UHRF1 epigenetically down-regulates UbcH8 to inhibit apoptosis in cervical cancer cells. Cell Cycle *17*, 300-308.